Magnetic and Nematic Orders of the Two-Dimensional Electron Gas at Oxide (111) Surfaces and Interfaces

Nazim Boudjada, Gideon Wachtel, and Arun Paramekanti
Department of Physics, University of Toronto, Toronto, Ontario M5S 1A7, Canada

(Received 1 June 2017; revised manuscript received 10 September 2017; published 23 February 2018)

Recent experiments have explored two-dimensional electron gases (2DEGs) at oxide (111) surfaces and interfaces, finding evidence for hexagonal symmetry breaking in $SrTiO_3$ at low temperature. We discuss many-body instabilities of such (111) 2DEGs, incorporating multiorbital interactions in the t_{2g} manifold which can induce diverse magnetic and orbital orders. Such broken symmetries may partly account for the observed nematicity, cooperating or competing with phonon mechanisms. We present an effective field theory for the interplay of magnetism and nematic charge order, and discuss implications of the nematicity for transport and superconductivity in (111) 2DEGs.

DOI: 10.1103/PhysRevLett.120.086802

Introduction.—Transition metal oxide heterostructures and interfaces can realize exotic low-dimensional electronic phases and allow for engineering oxide-based devices [1]. Extensive research [2–24] has focused on the two-dimensional electron gas (2DEG) at the (001) $LaAlO_3$-$SrTiO_3$ (LAO-STO) interface induced by a combination of the polar catastrophe and oxygen vacancies. This 2DEG shows evidence of correlated magnetism in torque magnetometry and scanning SQUID measurements [10,11]. In addition, it exhibits superconductivity (SC) [6,25] which may be tied to that of doped bulk STO, though the interface might harbor modulated SC pairing [26] or Majorana modes [27].

Recently, various groups have started to probe 2DEGs at oxide (111) surfaces and interfaces, for instance induced by photon [28] or ion [29,30] irradiation at the (111) STO surface, as well as that at the (111) LAO-STO interface [31–35]. Part of this interest stems from proposals for realizing topologically nontrivial phases along this growth direction [36–43]. The [111] growth direction is polar for STO due to alternating Ti^{4+} and $(SrO_3)^{4-}$ layers, and the internal electric fields could lead to stronger confinement [44] of the (111) 2DEG, potentially enhancing correlation effects relative to (001) 2DEGs. Angle resolved photoemission spectroscopy (ARPES) on the (111) STO surface reveals a Fermi surface (FS) composed of all three t_{2g} orbitals, which appears to preserve the expected hexagonal symmetry [28,29]. However, very recent experiments have discovered, via measurements of magnetotransport [30–33] and the resistive transition into the SC state [35], that this (111) 2DEG exhibits an anisotropy which sets in at low temperatures, spontaneously breaking the hexagonal symmetry. While a weak resistive anisotropy may arise from the ~100 K pseudocubic to pseudotetragonal transition of bulk STO [45], the onset temperature seen in these experiments is much lower, $T_{\mathrm{ani}} \sim 4$–30 K depending on the sample and the electron density. For bulk STO, it is known that the transition into the pseudotetragonal phase is sensitive to stress along the [111] direction [46], and proceeds via an intermediate trigonal phase; it remains to be tested if the lower symmetry at the (111) surface or interface leads to a low temperature surface phonon instability.

In light of these developments, it is in any case also important to consider the impact of electron-electron interactions on (111) 2DEGs, in order to (i) study possible interaction induced many-body instabilities, and (ii) ask if there are electronic mechanisms for the observed anisotropies of the (111) 2DEG which may cooperate or compete with phonon instabilities. Such an interplay has been actively investigated in the iron pnictide superconductors (see Ref. [47] for a review).

Motivated by these questions, we examine a model for t_{2g} electronic states of the (111) STO surface 2DEG, which is consistent with the ARPES measurements, and study its instabilities driven by multiorbital interactions. Our main findings, summarized in Figs. 1 and 2, based on a combination of random phase approximation (RPA) calculations supplemented by mean field theory, is that there is a range of densities over which this 2DEG is unstable to ferromagnetic (FM) or antiferromagnetic (AFM) order, accompanied by ferro-orbital order. Even if thermal fluctuations melt such magnetic orders in two dimensions, the orbital order and the fluctuating magnetism are expected to survive to higher temperatures, leading to a nematic fluid [48–53] which breaks hexagonal symmetry. We present a Landau theory of this nematic, and discuss implications for transport measurements and superconductivity. Such nematicity induced by orbital or spin order has been previously considered for the (001) 2DEG [23,54–56]. Our results should be broadly applicable to a wide class of oxide (111) 2DEGs.

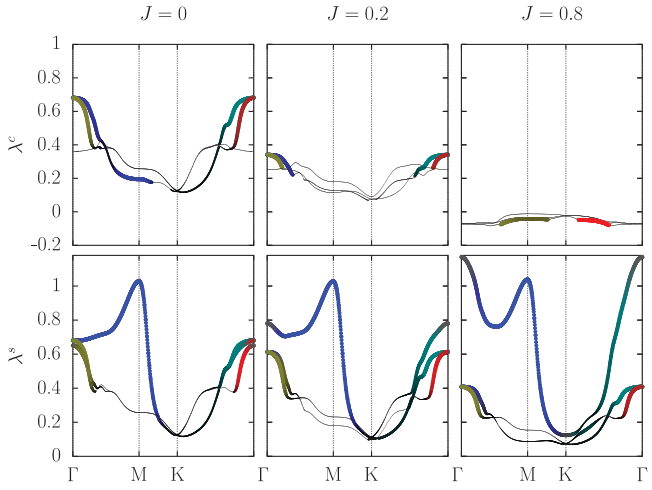

FIG. 1. The dominant three eigenvalues $\lambda^{(c,s)}$ (c = charge, s = spin) of the matrix product $\underline{U}^{(c,s)}\underline{\chi}_0(\mathbf{q},\Omega=0)$, plotted along high symmetry lines of the BZ, with $t=1$, $U=2$, $t_\perp=-t'=0.04$, and $T=0.02$, for fixed density $\bar{n}=0.3$, and varying Hund's coupling J/t. Line color (red, green, blue) indicates relative weight of orbitals (respectively, xy, xz, yz) in the orbital-diagonal part of the eigenvectors $|f^{(c,s)}_{\ell\ell}|^2$; thickness indicates total weight, $\sum_\ell |f^{(c,s)}_{\ell\ell}|^2$. The dominant instability is in the spin channel, being antiferromagnetic (near M) for small J and ferromagnetic (at Γ) for large J. In the charge channel, the leading instability at small J is a twofold degenerate mode at Γ corresponding to ferro-orbital order.

Model.—We begin with a tight-binding model of Ti t_{2g} orbitals on a 2D triangular lattice that captures the FS seen in ARPES [28,29] for the (111) 2DEG at the STO surface:

$$H_0 = \sum_{\mathbf{k}\ell\ell'\sigma} c^\dagger_{\ell\sigma}(\mathbf{k}) h_{\ell\ell'}(\mathbf{k}) c_{\ell'\sigma}(\mathbf{k}), \tag{1}$$

with $\ell \equiv yz,\ zx,\ xy$, and

$$\underline{h}(\mathbf{k}) = \begin{pmatrix} \epsilon^c_{\mathbf{k}} + \eta^{ab}_{\mathbf{k}} & \gamma^a_{\mathbf{k}} & \gamma^b_{\mathbf{k}} \\ \gamma^a_{\mathbf{k}} & \epsilon^b_{\mathbf{k}} + \eta^{ca}_{\mathbf{k}} & \gamma^c_{\mathbf{k}} \\ \gamma^b_{\mathbf{k}} & \gamma^c_{\mathbf{k}} & \epsilon^a_{\mathbf{k}} + \eta^{bc}_{\mathbf{k}} \end{pmatrix}, \tag{2}$$

where $\epsilon^\alpha_{\mathbf{k}} = -2t\cos k_\alpha$ and $\eta^{\alpha\beta}_{\mathbf{k}} = -2t_\perp(\cos k_\alpha + \cos k_\beta)$ determine the intraorbital dispersion which leads to elliptical FSs, while $\gamma^\alpha_{\mathbf{k}} = -2t'\cos k_\alpha$ captures weak interorbital hopping. Here we have defined $k_\alpha = \mathbf{k}\cdot\hat{\alpha}$ ($\alpha = a,\ b,\ c$), with $\hat{a} = \hat{x}$, $\hat{b} = \hat{x}/2 + \hat{y}\sqrt{3}/2$, and $\hat{c} = -\hat{x}/2 + \hat{y}\sqrt{3}/2$. We work in units where the triangular lattice constant d $\approx$ 5.66 Å is set to unity. The ARPES data [28,29] can be reasonably fit by choosing $t = 320$ meV and $t_\perp = 0.04t$, and an electron density of $\bar{n} = 0.3$ electrons per site, corresponding to 10^{14} cm^{-2}; we therefore study a range of densities around this value. The interorbital terms appear to be small; for concreteness, we set $t' = -0.04t$. The resulting FSs are shown overlaid on the paramagnetic phases in Fig. 2. The real 2DEG wave functions will be spread over a few layers, so H_0 should only be viewed as the simplest 2D tight-binding parametrization of the ARPES data. We omit spin-orbit coupling (SOC), but comment on its effects later. The local multiorbital interactions are

$$H_{\text{int}} = U\sum_{i\ell} n_{i\ell\uparrow}n_{i\ell\downarrow} + \frac{1}{2}V\sum_{i\ell\neq\ell'} n_{i\ell}n_{i\ell'} - J\sum_{i\ell\neq\ell'} \mathbf{S}_{i\ell}\cdot\mathbf{S}_{i\ell'} + J'\sum_{i\ell\neq\ell'} c^\dagger_{i\ell\uparrow}c^\dagger_{i\ell\downarrow}c_{i\ell'\downarrow}c_{i\ell'\uparrow}. \tag{3}$$

where i denotes the site and ℓ the orbital. Below, we fix $V = (U - 5J/2)$ and $J' = J$ as appropriate for t_{2g} orbitals, and explore broken symmetry states driven by varying the interactions J/t, U/t. These interactions should be scaled down compared to atomic values by the number of layers over which the 2DEG is spread.

RPA analysis.—To identify the leading weak-coupling instabilities we use an unbiased multiorbital RPA approach [57], with the matrix response $\underline{\chi}^{(c,s)}_{\text{RPA}}(\mathbf{q},\Omega) = \underline{\chi}_0(\mathbf{q},\Omega)[1 - \underline{U}^{(c,s)}\underline{\chi}_0(\mathbf{q},\Omega)]^{-1}$, where

$$(\underline{\chi}_0(\mathbf{q},\Omega))_{\ell_1\ell_2;\ell_3\ell_4} = \frac{1}{N}\sum_{ij\sigma\sigma'}\int_0^\beta d\tau e^{i\mathbf{q}\cdot(\mathbf{r}_i-\mathbf{r}_j)-i\Omega\tau} \times \langle c^\dagger_{i\ell_1\sigma}(\tau)c_{i\ell_2\sigma}(\tau)c^\dagger_{j\ell_3\sigma'}(0)c_{j\ell_4\sigma'}(0)\rangle \tag{4}$$

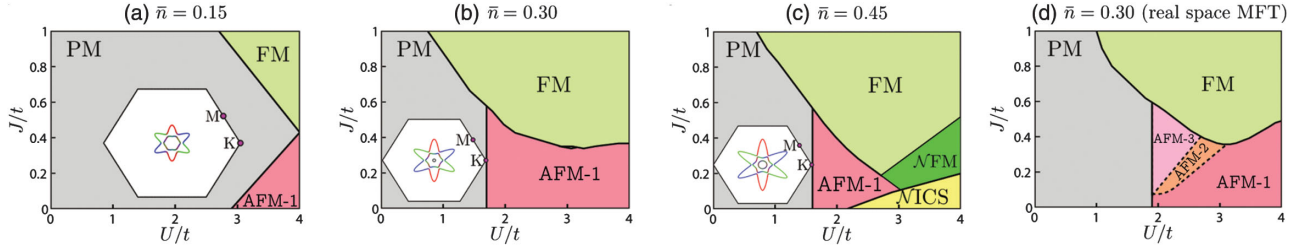

FIG. 2. Zero temperature phase diagram of the (111) 2DEG as a function of the Hubbard repulsion U/t and Hund's coupling J/t for densities (a) $\bar{n} = 0.15$, (b) $\bar{n} = 0.30$, (c) $\bar{n} = 0.45$ within a single-$\mathbf{Q}$ spiral mean field theory. The different metallic phases are the PM, AFM-1, ICS, and a FM phase at large Hund's coupling. The PM phases depict the noninteracting Fermi surfaces. (d) Real space MFT (at $\bar{n} = 0.3$, $T = 0.02t$) showing that the commensurate AFM order might support regimes of multi-$\mathbf{Q}$ orders (AFM-2, AFM-3). The $\mathcal{N}$FM, ICS, AFM-1, and AFM-2 phases coexist with ferro-orbital order which will lead to transport anisotropies.

is the bare response function (see the Supplemental Material [58]). Here, N is the number of sites, c and s, respectively, denote charge and spin responses. The nonzero interaction vertex matrices are

$$(U^c)_{\ell\ell;\ell\ell} = -U, \qquad (U^c)_{\ell\ell';\ell\ell'} = -2V,$$
$$(U^c)_{\ell\ell;\ell'\ell'} = V - \frac{3}{2}J, \qquad (U^c)_{\ell\ell';\ell'\ell} = -2J', \tag{5}$$

$$(U^s)_{\ell\ell;\ell\ell} = U, \qquad (U^s)_{\ell\ell';\ell\ell'} = J,$$
$$(U^s)_{\ell\ell;\ell'\ell'} = \frac{1}{2}J - V, \qquad (U^s)_{\ell\ell';\ell'\ell} = 2J', \tag{6}$$

where $\ell \neq \ell'$. When the largest eigenvalue of $\underline{U}^{(c,s)}\underline{\chi}_0(\mathbf{q}, \Omega = 0)$ is $\lambda^{(c,s)}(\mathbf{q}) = 1$, the response function diverges, indicating an instability towards an ordered state, with corresponding eigenvectors, $f^{(c,s)}_{\ell\ell'}(\mathbf{q})$. Figure 1 shows the largest eigenvalues, $\lambda^c(\mathbf{q})$ and $\lambda^s(\mathbf{q})$, along high symmetry lines in the Brillouin zone (BZ) for $\bar{n} = 0.3$, $U/t = 2$, and temperature $T/t = 0.02$, demonstrating the emergence of various instabilities as we vary Hund's coupling. For our choice of experimentally motivated parameters, the leading instabilities are nearly orbital diagonal, $f^{(c,s)}_{\ell\ell'}(\mathbf{q}) \approx f^{(c,s)}_{\ell}(\mathbf{q})\delta_{\ell\ell'}$.

When $J = 0$, the Hubbard interaction U drives a leading instability in the spin channel, with $\mathbf{q}$ generically incommensurate (close to the M points of the BZ for the range of densities investigated), with all the weight on a single orbital. This instability indicates a tendency towards incommensurate spiral or commensurate stripe antiferromagnetic order—for each orbital in a different direction. In the charge channel, we find a subleading instability, with two degenerate eigenvalues at $\mathbf{q} = 0$, indicating a tendency towards ferro-orbital order which will lead to nematicity associated with broken lattice rotational symmetry. With increasing J, the AFM instability gives way to a ferromagnetic instability seen in the spin response at the Γ point. At the same time, the ferro-orbital response is strongly suppressed. Below, we use mean field theory (MFT) in order to further characterize the broken symmetry phases.

Mean field theory.—We study the phase diagram of our model, Eqs. (1)–(3), using a momentum space MFT within a single-$\mathbf{Q}$ spiral ansatz with a spatially uniform but orbital-dependent density. This is captured by a Hamiltonian, $H_{\text{var}} = H_0 - \sum_{i\ell}(\phi_\ell + \mu)n_{i\ell} - \sum_{i\ell}\mathbf{b}_\ell \cdot \mathbf{S}_{i\ell}e^{i\mathbf{Q}\cdot\mathbf{r}_i}$, which we use to generate variational ground states $|\psi_{\text{var}}\rangle$ at the desired charge density by tuning μ. The fields ϕ_ℓ, $\mathbf{b}_\ell$, and the wave vector $\mathbf{Q}$ are selected to minimize $\langle\psi_{\text{var}}|H_0 + H_{\text{int}}|\psi_{\text{var}}\rangle$ (see the Supplemental Material [58]).

Figures 2(a)–2(c) shows the MFT phase diagrams for densities $\bar{n} = 0.15$, 0.30, 0.45. Broadly, we find three phases consistent with RPA: (i) a paramagnetic (PM) metal where $\phi_\ell = 0$, $\mathbf{b}_\ell = 0$, (ii) a commensurate stripe-AFM (AFM-1) or incommensurate spiral (ICS) metal driven by U, where $\phi_\ell \neq 0$ and $\mathbf{b}_\ell \neq 0$, which has higher density in one of the three orbitals, and (iii) a FM metal driven by Hund's coupling where $\mathbf{b}_\ell = \mathbf{b}$, and $\mathbf{Q} = 0$, either having the same density in all orbitals (FM), or with one orbital having a lower density than the other two (i.e., a nematic FM: $\mathcal{N}$FM). Interestingly, we find a direct (generically first-order) transition from the PM into the AFM-1 phase for all three densities, in contrast to the RPA which finds AFM-1 only at a fine-tuned density.

To go beyond the single-$\mathbf{Q}$ ansatz, we have also studied the commensurate AFM order by minimizing the free energy at $T = 0.02t$ assuming a 2×2 unit cell. The result for $\bar{n} = 0.3$ is shown in Fig. 2(d) (see also the Supplemental Material [58]); we find reasonably good agreement with the single-$\mathbf{Q}$ MFT, but discover small regimes where the single-$\mathbf{Q}$ order gives way to multi-$\mathbf{Q}$ condensates where two (AFM-2) or three (AFM-3) wave vectors are simultaneously present. A robust feature is the presence of simultaneous AFM and ferro-orbital order in the AFM-1 and AFM-2 phases. A similar competition between single-$\mathbf{Q}$ and multi-$\mathbf{Q}$ phases also appears in single-orbital honeycomb and triangular lattice Hubbard models [59,60].

The $\mathcal{N}$FM, AFM-1, AFM-2, and ICS phases feature discrete ferro-orbital order which breaks the hexagonal lattice symmetry. Thus, even if fluctuations melt the magnetic order itself, there may be large regimes in the phase diagram where the electronic nematicity survives. Below we use Landau theory to further understand this interplay of magnetism and nematicity.

Effective field theory.—Landau theory is a powerful tool to analyze magnetic orders [17] and study spin textures such as Skyrmions, which might arise at the (001) LAO-STO interface [56]. For the (111) 2DEG, our RPA analysis suggests that the soft electronic modes include a complex nematic charge mode $\psi_n = \delta\rho_{xy} + \omega\delta\rho_{yz} + \omega^2\delta\rho_{zx}$ (with $\omega = e^{i2\pi/3}$) constructed from the slowly varying orbital densities $\delta\rho_\ell$ at the Γ point, and the spin modes, $\vec{\varphi}_0$ at the Γ point, and $\vec{\varphi}_\alpha$ at the magnetic wave vectors $\mathbf{Q}_\alpha$ ($\alpha = 1$, 2, 3), which can describe both FM and AFM orders. Since the interorbital hopping is small, $\vec{\varphi}_{1,2,3} \sim \vec{\varphi}_{xy,yz,zx}$ but with weak orbital admixture. The spin modes $\vec{\varphi}_\alpha$ are complex for incommensurate $\mathbf{Q}_\alpha$, and real if $\mathbf{Q}_\alpha$ corresponds to the commensurate M points. The nematic order parameter ψ_n transforms under anticlockwise lattice $\pi/3$ rotations as $\psi_n \to \omega^2\psi_n$, and under reflections about the $\hat{x}$ axis as $\psi_n \to \psi_n^*$. Turning to the spin modes, $\vec{\varphi}_0$ is invariant under lattice symmetries, anticlockwise $\pi/3$ rotations lead to $\vec{\varphi}_1 \to \vec{\varphi}_2$, $\vec{\varphi}_2 \to \vec{\varphi}_3$, $\vec{\varphi}_3 \to \vec{\varphi}_1^*$. Under spin rotations, ψ_n is invariant but all spin modes undergo $SO(3)$ rotations, $\vec{\varphi}_{0,\alpha} \to \mathfrak{R}\vec{\varphi}_{0,\alpha}$. Time reversal sends $\vec{\varphi}_{0,\alpha} \to -\vec{\varphi}_{0,\alpha}$. Armed with this, the mean field Landau free energy is $\mathcal{F} = \int d^2x(\mathcal{L}_\psi + \mathcal{L}_\varphi + \mathcal{L}_{\psi\varphi})$, with

$$\mathcal{L}_\psi = r_\psi|\psi_n|^2 + w_\psi(\psi_n^3 + \psi_n^{*3}) + u_\psi|\psi_n|^4 + \ldots, \quad (7)$$

$$\mathcal{L}_\varphi = r_0\vec{\varphi}_0 \cdot \vec{\varphi}_0 + r_Q\sum_\alpha|\vec{\varphi}_\alpha|^2 + \ldots, \quad (8)$$

$$\mathcal{L}_{\psi\varphi} = -\lambda_1(\psi_n^*\mathcal{S}_n + \psi_n\mathcal{S}_n^*) - \lambda_2|\vec{\varphi}_0|^2|\psi_n|^2, \quad (9)$$

where we have defined a complex magnetic nematic order $\mathcal{S}_n = |\vec{\varphi}_1|^2 + \omega|\vec{\varphi}_2|^2 + \omega^2|\vec{\varphi}_3|^2$, which transforms analogous to ψ_n. In this effective field theory, the PM phase corresponds to $(r_\psi, r_0, r_Q > 0)$, the FM phase corresponds to $(r_0 < 0, r_\psi, r_Q > 0)$, and the various AF phases correspond to $(r_Q < 0, r_0 > 0)$. Note that we never find a ground state nematic charge order unaccompanied by spin order in the MFT. The various types of AF orders will be dictated by higher order (quartic and sixth order) terms denoted above by ellipses. In turn, this can lead to a "pinning field" for the charge nematic order via the cubic interaction λ_1 in $\mathcal{L}_{\psi\varphi}$; our mean field results indicate $w_\psi, \lambda_1, \lambda_2 > 0$. Below, we discuss some implications of this Landau theory, deferring its microscopic derivation to a future publication.

(a) Incommensurate spiral (ICS)—For the generic incommensurate instability, the simplest spin order (which will not lead to any charge modulation) is a single-mode coplanar spiral at one $\mathbf{Q}_\alpha$, with the complex $\vec{\varphi}_\alpha = \hat{\Omega}_1 + i\hat{\Omega}_2$ and $\hat{\Omega}_1 \cdot \hat{\Omega}_2 = 0$. This leads to $\mathcal{S}_n \sim \omega^{\alpha-1}$, so the cubic interaction $\lambda_1 > 0$ will pin $\psi_n \sim \omega^{\alpha-1}$, causing density enhancement in orbital α.

(b) Commensurate AFM order—For commensurate stripe AFM order, $\mathbf{Q}_\alpha \equiv M_\alpha$, in which case $\vec{\varphi}_\alpha$ are real fields. This case, for which we have also carried out a real space MFT, leads to three orders. (i) AFM-1 has condensation at a single M_α, which corresponds to a collinear stripe order with $\vec{\varphi}_\alpha \sim \hat{\Omega}_1$. This has $\mathcal{S}_n \sim \omega^{\alpha-1}$, which pins $\psi_n \sim \omega^{\alpha-1}$, leading to a charge nematic order similar to the ICS state. (ii) AFM-2 features condensation at a pair of wave vectors M_α, M_β, with $\langle\vec{\varphi}_\alpha\rangle \sim \hat{\Omega}_1$ and $\langle\vec{\varphi}_\beta\rangle \sim \hat{\Omega}_2$. This state can be either collinear, $\hat{\Omega}_1 = \hat{\Omega}_2$, or coplanar, $\hat{\Omega}_1 \cdot \hat{\Omega}_2 = 0$. In both cases, however, $\mathcal{S}_n, \psi_n \sim \omega^{\alpha-1} + \omega^{\beta-1}$, displaying charge nematic order. (iii) Finally, AFM-3 is a triple-$\mathbf{Q}$ spin crystal, similarly featuring either collinear or noncoplanar tetrahedral order of the spins. Both cases are obtained by condensation at all three M points, with $\langle\vec{\varphi}_{1,2,3}\rangle \sim \hat{\Omega}_{1,2,3}$, and $\mathcal{S}_n = 0$, so no charge nematic is induced. In the collinear case $\hat{\Omega}_1 = \hat{\Omega}_2 = \hat{\Omega}_3$, while in the noncoplanar spin order $\hat{\Omega}_1 \cdot \hat{\Omega}_2 = 0$, and $\hat{\Omega}_3 = \pm\hat{\Omega}_1 \times \hat{\Omega}_2$. The latter case, in the presence of interorbital hopping, will feature an anomalous Hall effect [61,62]. The collinear AFM-2 and AFM-3 will also break translational symmetries with associated charge modulation driven by terms proportional to $\vec{\varphi}_\alpha \cdot \vec{\varphi}_\beta \neq 0$; such orders may be favored by repulsive interactions between neighboring sites.

(c) Nematic FM ($\mathcal{N}$FM) order—Starting with a uniform FM state, the quartic coupling $\lambda_2 > 0$, if sufficiently large, can drive charge nematicity, since it can change the "mass" of the nematic field to $(r_\psi - \lambda_2|\vec{\varphi}_0|^2)$. This coupling between FM and nematic orders is not linear in ψ_n, unlike the above AFM/ICS cases. Thus, the nematicity in this case is not symmetry enforced. For $w_\psi > 0$, the $\mathcal{N}$FM will have depletion of the density in one orbital, as we find from the MFT.

Fluctuation-disorder effects.—In two dimensions, without SOC, thermal fluctuations will destroy long-range magnetic order at any $T > 0$. In this case, ICS, the $\mathcal{N}$FM, the collinear AFM-1, and orthogonal AFM-2, will melt into a charge nematic, reflected in a nonzero ψ_n, $\mathcal{S}_n$, which will undergo symmetry restoration via a Z_3 clock (or 3-state Potts) transition. Within MFT this is a first order transition, but thermal fluctuations render it a continuous transition [63]. The noncoplanar AFM-3 state will lead to a magnetically melted state with only chiral order (linked to the $\pm$ choice of $\hat{\Omega}_3$), featuring a nonzero anomalous Hall effect that vanishes above an Ising transition at which time-reversal symmetry is restored [62].

We speculate that disorder might also weakly suppress long-range magnetic order, even with SOC, leaving vestigial nematic order [64] down to $T = 0$. This suggestion is motivated by $Sr_3Ru_2O_7$, where the observation of nematic transport [65] near the metamagnetic critical point was recently attributed, via neutron scattering, to arise from *nearly* ordered SDW phases [66].

Discussion.—The electronic nematic phases we have proposed in (111) 2DEGs will lead to transport anisotropies. On symmetry grounds, the scaled resistive anisotropy $(\rho_{xx} - \rho_{yy})/(\rho_{xx} + \rho_{yy})$ will track the nematic order parameter [67,68]. A simple Drude picture (see the Supplemental Material [58]) shows that, for the coordinates used above, $\rho_{xx} - \rho_{yy} \sim \mathrm{Re}\psi_n$ while $\rho_{xy} = \rho_{yx} \sim \mathrm{Im}\psi_n$. Further signatures of nematic order may be observed in Friedel oscillations which can be probed using scanning tunneling spectroscopy. Even in a conventional phonon-induced SC state, the presence of such background nematic order would lead to an anisotropy of the vortex shape and the mobility as well as the critical current, explaining the anisotropy observed in the resistive transition into the SC state [35]. If such orbital order is weak, it will be less evident in ARPES [28,29] than in transport probes.

Rashba SOC [14,69–71] does not significantly impact the (111) FS for relevant densities $\bar{n} \sim 0.3$, or lead to a significant spin splitting near the tips of the elliptical FSs where we find the magnetic instability (see the Supplemental Material [58]) since orbital mixing is negligible at those momenta. Thus, we expect SOC will not significantly modify the phase diagram at these densities; however, it can pin the magnetic order or convert the uniform FM into a long wavelength spiral [17,56]. SOC will have a more significant impact on low density 2DEGs,

and transport properties which average over the entire FS of all bands.

Our work has not taken into account random oxygen vacancies—these can locally pin the nematic order but cannot induce anisotropies in macroscopically averaged resistivity measurements. However, such "nematogen" defects could amplify weak resistive anisotropies, both of the bulk tetragonal phase in dilute 2DEGs, as well as of the higher density nematic phases with orbital order. This interplay, which has been studied in the pnictides [72], would be worth exploring in the oxide 2DEGs.

Finally, tetragonal lattice distortions, described by a three-state Potts theory [45] similar to $\mathcal{L}_\psi$, will couple linearly to the nematic order parameter ψ_n itself, affecting the SDW degrees of freedom as well. For instance, a tetragonal distortion with elongation of the c axis will favor the nematic order associated with the AFM-1 state. The interplay of electronic nematicity explored here, with anisotropies induced by surface phonon mechanisms, is an important topic for future research.

We thank F. Y. Bruno, Q. Li, L. Miao, A. Chubukov, and E. Fradkin for useful discussions and feedback. This research was supported by NSERC of Canada. A. P. acknowledges the support and hospitality of the International Center for Theoretical Sciences (Bangalore) during completion of this manuscript.

[1] J. Chakhalian, J. W. Freeland, A. J. Millis, C. Panagopoulos, and J. M. Rondinelli, Colloquium, Rev. Mod. Phys. **86**, 1189 (2014).

[2] A. Ohtomo and H. Y. Hwang, A high-mobility electron gas at the $LaAlO_3/SrTiO_3$ heterointerface, Nature (London) **427**, 423 (2004).

[3] S. Thiel, G. Hammerl, A. Schmehl, C. W. Schneider, and J. Mannhart, Tunable quasi-two-dimensional electron gases in oxide heterostructures, Science **313**, 1942 (2006).

[4] N. Nakagawa, H. Y. Hwang, and D. A. Muller, Why some interfaces cannot be sharp, Nat. Mater. **5**, 204 (2006).

[5] M. Takizawa, H. Wadati, K. Tanaka, M. Hashimoto, T. Yoshida, A. Fujimori, A. Chikamatsu, H. Kumigashira, M. Oshima, K. Shibuya, T. Mihara, T. Ohnishi, M. Lippmaa, M. Kawasaki, H. Koinuma, S. Okamoto, and A. J. Millis, Photoemission from Buried Interfaces in $LaAlO_3/SrTiO_3$ Superlattices, Phys. Rev. Lett. **97**, 057601 (2006).

[6] N. Reyren, S. Thiel, A. D. Caviglia, L. Fitting Kourkoutis, G. Hammerl, C. Richter, C. W. Schneider, T. Kopp, A.-S. Rüetschi, D. Jaccard, M. Gabay, D. A. Muller, J.-M. Triscone, and J. Mannhart, Superconducting interfaces between insulating oxides, Science **317**, 1196 (2007).

[7] A. D. Caviglia, S. Gariglio, N. Reyren, D. Jaccard, T. Schneider, M. Gabay, S. Thiel, G. Hammerl, J. Mannhart, and J.-M. Triscone, Electric field control of the $LaAlO_3/SrTiO_3$ interface ground state, Nature (London) **456**, 624 (2008).

[8] A. D. Caviglia, M. Gabay, S. Gariglio, N. Reyren, C. Cancellieri, and J.-M. Triscone, Tunable Rashba Spin-Orbit Interaction at Oxide Interfaces, Phys. Rev. Lett. **104**, 126803 (2010).

[9] Ariando, X. Wang, G. Baskaran, Z. Q. Liu, J. Huijben, J. B. Yi, A. Annadi, A. Roy Barman, A. Rusydi, S. Dhar, Y. P. Feng, J. Ding, H. Hilgenkamp, and T. Venkatesan, Electronic phase separation at the $LaAlO_3/SrTiO_3$ interface, Nat. Commun. **2**, 188 (2011).

[10] J. A. Bert, B. Kalisky, C. Bell, M. Kim, Y. Hikita, H. Y. Hwang, and K. A. Moler, Direct imaging of the coexistence of ferromagnetism and superconductivity at the $LaAlO_3/SrTiO_3$ interface, Nat. Phys. **7**, 767 (2011).

[11] L. Li, C. Richter, J. Mannhart, and R. C. Ashoori, Coexistence of magnetic order and two-dimensional superconductivity at $LaAlO_3/SrTiO_3$ interfaces, Nat. Phys. **7**, 762 (2011).

[12] G. Khalsa and A. H. MacDonald, Theory of the $SrTiO_3$ surface state two-dimensional electron gas, Phys. Rev. B **86**, 125121 (2012).

[13] M. M. Mehta, D. A. Dikin, C. W. Bark, S. Ryu, C. M. Folkman, C. B. Eom, and V. Chandrasekhar, Evidence for charge-vortex duality at the $LaAlO_3/SrTiO_3$ interface, Nat. Commun. **3**, 955 (2012).

[14] Z. Zhong, A. Tóth, and K. Held, Theory of spin-orbit coupling at $LaAlO_3/SrTiO_3$ interfaces and $SrTiO_3$ surfaces, Phys. Rev. B **87**, 161102 (2013).

[15] M. H. Fischer, S. Raghu, and E.-A. Kim, Spin-orbit coupling in $LaAlO_3/SrTiO_3$ interfaces: Magnetism and orbital ordering, New J. Phys. **15**, 023022 (2013).

[16] Y. Kim, R. M. Lutchyn, and C. Nayak, Origin and transport signatures of spin-orbit interactions in one- and two-dimensional $SrTiO_3$-based heterostructures, Phys. Rev. B **87**, 245121 (2013).

[17] S. Banerjee, O. Erten, and M. Randeria, Ferromagnetic exchange, spin-orbit coupling and spiral magnetism at the $LaAlO_3/SrTiO_3$ interface, Nat. Phys. **9**, 626 (2013).

[18] G. Chen and L. Balents, Ferromagnetism in Itinerant Two-Dimensional t_{2g} Systems, Phys. Rev. Lett. **110**, 206401 (2013).

[19] S. Y. Park and A. J. Millis, Charge density distribution and optical response of the $LaAlO_3/SrTiO_3$ interface, Phys. Rev. B **87**, 205145 (2013).

[20] J. Ruhman, A. Joshua, S. Ilani, and E. Altman, Competition Between Kondo screening and magnetism at the $LaAlO_3/SrTiO_3$ interface, Phys. Rev. B **90**, 125123 (2014).

[21] M. Diez, A. M. R. V. L. Monteiro, G. Mattoni, E. Cobanera, T. Hyart, E. Mulazimoglu, N. Bovenzi, C. W. J. Beenakker, and A. D. Caviglia, Giant Negative Magnetoresistance Driven by Spin-Orbit Coupling at the $LaAlO_3/SrTiO_3$ Interface, Phys. Rev. Lett. **115**, 016803 (2015).

[22] S. Nandy, N. Mohanta, S. Acharya, and A. Taraphder, Anomalous transport near the Lifshitz transition at the $LaAlO_3/SrTiO_3$ interface, Phys. Rev. B **94**, 155103 (2016).

[23] J. R. Tolsma, M. Polini, and A. H. MacDonald, Orbital and spin order in oxide two-dimensional electron gases, Phys. Rev. B **95**, 205101 (2017).

[24] W. A. Atkinson, P. Lafleur, and A. Raslan, Influence of the ferroelectric quantum critical point on $SrTiO_3$ interfaces, Phys. Rev. B **95**, 054107 (2017).

[25] D. A. Dikin, M. Mehta, C. W. Bark, C. M. Folkman, C. B. Eom, and V. Chandrasekhar, Coexistence of

Superconductivity and Ferromagnetism in Two Dimensions, Phys. Rev. Lett. **107**, 056802 (2011).

[26] K. Michaeli, A. C. Potter, and P. A. Lee, Superconducting and Ferromagnetic Phases in $SrTiO_3/LaAlO_3$ Oxide Interface Structures: Possibility of Finite Momentum Pairing, Phys. Rev. Lett. **108**, 117003 (2012).

[27] L. Fidkowski, H.-C. Jiang, R. M. Lutchyn, and C. Nayak, Magnetic and superconducting ordering in one-dimensional nanostructures at the $LaAlO_3/SrTiO_3$ interface, Phys. Rev. B **87**, 014436 (2013).

[28] T. C. Rödel, C. Bareille, F. Fortuna, C. Baumier, F. Bertran, P. Le Févre, M. Gabay, O. Hijano Cubelos, M. J. Rozenberg, T. Maroutian, P. Lecoeur, and A. F. Santander-Syro, Orientational Tuning of the Fermi Sea of Confined Electrons at the $SrTiO_3$ (110) and (111) Surfaces, Phys. Rev. Applied **1**, 051002 (2014).

[29] S. McKeown Walker, A. de la Torre, F. Y. Bruno, A. Tamai, T. K. Kim, M. Hoesch, M. Shi, M. S. Bahramy, P. D. C. King, and F. Baumberger, Control of a Two-Dimensional Electron Gas on $SrTiO_3$ (111) by Atomic Oxygen, Phys. Rev. Lett. **113**, 177601 (2014).

[30] L. Miao, R. Du, Y. Yin, and Q. Li, Anisotropic magnetotransport properties of electron gases at $SrTiO_3$ (111) and (110) surfaces, Appl. Phys. Lett. **109**, 261604 (2016).

[31] P. K. Rout, I. Agireen, E. Maniv, M. Goldstein, and Y. Dagan, Six-fold crystalline anisotropic magnetoresistance in (111) $LaAlO_3/SrTiO_3$ oxide interface, Phys. Rev. B **95**, 241107 (2017).

[32] S. Davis, V. Chandrasekhar, Z. Huang, K. Han, Ariando, and T. Venkatesan, Anisotropic multicarrier transport at the (111) $LaAlO_3/SrTiO_3$ interface, Phys. Rev. B **95**, 035127 (2017).

[33] S. K. Davis, Z. Huang, K. Han, Ariando, T. Venkatesan, and V. Chandrasekhar, Electrical transport anisotropy controlled by oxygen vacancy concentration in (111) $LaAlO_3/SrTiO_3$ interface structures, Adv. Mater. Interfaces **4**, 1600830 (2017).

[34] A. M. R. V. L. Monteiro, D. J. Groenendijk, I. Groen, J. de Bruijckere, R. Gaudenzi, H. S. J. van der Zant, and A. D. Caviglia, Two-dimensional superconductivity at the (111) $LaAlO_3/SrTiO_3$ interface, Phys. Rev. B **96**, 020504 (2017).

[35] S. Davis, Z. Huang, K. Han, Ariando, T. Venkatesan, and V. Chandrasekhar, Superconductivity and Frozen Electronic States at the (111) $LaAlO_3/SrTiO_3$ Interface, arXiv: 1704.01203.

[36] D. Xiao, W. Zhu, Y. Ran, N. Nagaosa, and S. Okamoto, Interface engineering of quantum hall effects in digital transition metal oxide heterostructures, Nat. Commun. **2**, 596 (2011).

[37] A. Rüegg and G. A. Fiete, Topological insulators from complex orbital order in transition-metal oxides heterostructures, Phys. Rev. B **84**, 201103 (2011).

[38] A. M. Cook and A. Paramekanti, Double perovskite heterostructures: Magnetism, Chern Bands, and Chern Insulators, Phys. Rev. Lett. **113**, 077203 (2014).

[39] S. Okamoto, W. Zhu, Y. Nomura, R. Arita, D. Xiao, and N. Nagaosa, Correlation effects in (111) bilayers of perovskite transition-metal oxides, Phys. Rev. B **89**, 195121 (2014).

[40] X. Hu, Z. Zhong, and G. A. Fiete, First principles prediction of topological phases in thin films of pyrochlore iridates, Sci. Rep. **5**, 11072 (2015).

[41] S. Baidya, U. V. Waghmare, A. Paramekanti, and T. Saha-Dasgupta, High-temperature large-gap quantum anomalous Hall insulating state in ultrathin double perovskite films, Phys. Rev. B **94**, 155405 (2016).

[42] L. Si, O. Janson, G. Li, Z. Zhong, Z. Liao, G. Koster, and K. Held, Quantum Anomalous Hall State in Ferromagnetic $SrRuO_3$ (111) Bilayers, Phys. Rev. Lett. **119**, 026402 (2017).

[43] H.-S. Kim and H.-Y. Kee, Realizing Haldane model in Fe-based honeycomb ferromagnetic insulators, npj Quantum Mater. **2**, 20 (2017).

[44] S. Baidya, U. V. Waghmare, A. Paramekanti, and T. Saha-Dasgupta, Controlled confinement of half-metallic two-dimensional electron gas in $BaTiO_3/Ba_2FeReO_6/BaTiO_3$ heterostructures: A first-principles study, Phys. Rev. B **92**, 161106 (2015).

[45] A. Aharony, K. A. Müller, and W. Berlinger, Trigonal-to-Tetragonal Transition in Stressed $SrTiO_3$: A Realization of the Three-State Potts Model, Phys. Rev. Lett. **38**, 33 (1977).

[46] K. Alex Müller, W. Berlinger, and E. Tosatti, Indication for a novel phase in the quantum paraelectric regime of $SrTiO_3$, Z. Phys. B **84**, 277 (1991).

[47] R. M. Fernandes, A. V. Chubukov, and J. Schmalian, What drives nematic order in iron-based superconductors?, Nat. Phys. **10**, 97 (2014).

[48] V. Oganesyan, S. A. Kivelson, and E. Fradkin, Quantum theory of a nematic Fermi fluid, Phys. Rev. B **64**, 195109 (2001).

[49] I. Khavkine, C.-H. Chung, V. Oganesyan, and H.-Y. Kee, Formation of an electronic nematic phase in interacting fermion systems, Phys. Rev. B **70**, 155110 (2004).

[50] H.-Y. Kee and Y. B. Kim, Itinerant metamagnetism induced by electronic nematic order, Phys. Rev. B **71**, 184402 (2005).

[51] E. Fradkin, S. A. Kivelson, and V. Oganesyan, Electron nematic phase in a transition metal oxide, Science **315**, 196 (2007).

[52] C. Fang, H. Yao, W.-F. Tsai, J. Hu, and S. A. Kivelson, Theory of electron nematic order in LaFeAsO, Phys. Rev. B **77**, 224509 (2008).

[53] E. Fradkin, S. A. Kivelson, M. J. Lawler, J. P. Eisenstein, and A. P. Mackenzie, Nematic Fermi fluids in condensed matter physics, Annu. Rev. Condens. Matter Phys. **1**, 153 (2010).

[54] J. Zhou, W.-Y. Shan, and D. Xiao, Spin responses and effective Hamiltonian for the two-dimensional electron gas at the oxide interface $LaAlO_3/SrTiO_3$, Phys. Rev. B **91**, 241302 (2015).

[55] M. H. Fischer, S. Raghu, and E.-A. Kim, Spin-orbit coupling in $LaAlO_3/SrTiO_3$ interfaces: magnetism and orbital ordering, New J. Phys. **15**, 023022 (2013).

[56] X. Li, W. V. Liu, and L. Balents, Spirals and Skyrmions in Two Dimensional Oxide Heterostructures, Phys. Rev. Lett. **112**, 067202 (2014).

[57] S. Graser, T. A. Maier, P. J. Hirschfeld, and D. J. Scalapino, Near-degeneracy of several pairing channels in multiorbital

models for the Fe pnictides, New J. Phys. **11**, 025016 (2009).

[58] See Supplemental Material at http://link.aps.org/supplemental/10.1103/PhysRevLett.120.086802 for (i) details of RPA calculations at different densities, (ii) the form and impact of Rashba SOC, (iii) details of mean field calculations, and (iv) transport nematicity within a Drude-type model.

[59] G.-W. Chern, R. M. Fernandes, R. Nandkishore, and A. V. Chubukov, Broken translational symmetry in an emergent paramagnetic phase of graphene, Phys. Rev. B **86**, 115443 (2012).

[60] R. Nandkishore, G.-W. Chern, and A. V. Chubukov, Itinerant Half-Metal Spin-Density-Wave State on the Hexagonal Lattice, Phys. Rev. Lett. **108**, 227204 (2012).

[61] I. Martin and C. D. Batista, Itinerant Electron-Driven Chiral Magnetic Ordering and Spontaneous Quantum Hall Effect in Triangular Lattice Models, Phys. Rev. Lett. **101**, 156402 (2008).

[62] Y. Kato, I. Martin, and C. D. Batista, Stability of the Spontaneous Quantum Hall State in the Triangular Kondo-Lattice Model, Phys. Rev. Lett. **105**, 266405 (2010).

[63] F. Y. Wu, The Potts model, Rev. Mod. Phys. **54**, 235 (1982).

[64] L. Nie, G. Tarjus, and S. A. Kivelson, Quenched disorder and vestigial nematicity in the pseudogap regime of the cuprates, Proc. Natl. Acad. Sci. U.S.A. **111**, 7980 (2014).

[65] R. A. Borzi, S. A. Grigera, J. Farrell, R. S. Perry, S. J. S. Lister, S. L. Lee, D. A. Tennant, Y. Maeno, and A. P. Mackenzie, Formation of a nematic fluid at high fields in $Sr_3Ru_2O_7$, Science **315**, 214 (2007).

[66] C. Lester, S. Ramos, R. S. Perry, T. P. Croft, R. I. Bewley, T. Guidi, P. Manuel, D. D. Khalyavin, E. M. Forgan, and S. M. Hayden, Field-tunable spin-density-wave phases in $Sr_3Ru_2O_7$, Nat. Mater. **14**, 373 (2015).

[67] E. Fradkin, S. A. Kivelson, E. Manousakis, and K. Nho, Nematic Phase of the Two-Dimensional Electron Gas in a Magnetic Field, Phys. Rev. Lett. **84**, 1982 (2000).

[68] S. Basak and E. W. Carlson, Distinguishing XY from Ising electron nematics, Phys. Rev. B **96**, 081303 (2017).

[69] J.-H. Park, C. H. Kim, H.-W. Lee, and J. H. Han, Orbital chirality and Rashba interaction in magnetic bands, Phys. Rev. B **87**, 041301 (2013).

[70] J.-H. Park, C. H. Kim, J.-W. Rhim, and J. H. Han, Orbital Rashba effect and its detection by circular dichroism angle-resolved photoemission spectroscopy, Phys. Rev. B **85**, 195401 (2012).

[71] S. R. Park, C. H. Kim, J. Yu, J. H. Han, and C. Kim, Orbital-Angular-Momentum Based Origin of Rashba-Type Surface Band Splitting, Phys. Rev. Lett. **107**, 156803 (2011).

[72] M. N. Gastiasoro, I. Paul, Y. Wang, P. J. Hirschfeld, and B. M. Andersen, Emergent Defect States as a Source of Resistivity Anisotropy in the Nematic Phase of Iron Pnictides, Phys. Rev. Lett. **113**, 127001 (2014).